Composition dependence of optical phonon energies and Raman line broadening in hexagonal $Al_xGa_{1-x}N$ alloys

V. Yu. Davydov,* I. N. Goncharuk, A. N. Smirnov, A. E. Nikolaev, W. V. Lundin, and A. S. Usikov
Ioffe Physico-Technical Institute, 194021 St. Petersburg, Russia

A. A. Klochikhin
Petersburg Nuclear Physics Institute, Gatchina, 188350 St. Petersburg, Russia

J. Aderhold, J. Graul, and O. Semchinova
LFI, Universität Hannover, Schneiderberg 32, 30167 Hannover, Germany

H. Harima
Department of Electronics and Information Science, Kyoto Institute of Technology, Matsugasaki, Sakyo-ku, Kyoto 606-8585, Japan
(Received 17 August 2001; revised manuscript received 19 October 2001; published 11 March 2002)

Studies of first- and second-order Raman scattering in hexagonal $Al_xGa_{1-x}N$ alloys are reported. The dependences of frequencies of all Raman-allowed optical phonons versus Al content are traced in detail in the entire composition range. The one-mode behavior of LO phonons and the two-mode behavior of the other phonons is established. It is shown that the composition dependences of A_1(TO), A_1(LO), E_1(LO), and E_2(low) phonon energies are convenient tools for the quantitative characterization of the Al content in $Al_xGa_{1-x}N$ alloys. The energy position of the B_1(high) silent mode is proposed. A narrow gap separating the dispersion regions of transverse and longitudinal optical phonons is revealed in the phonon density-of-state function. The composition dependence of the phonon line broadening is investigated experimentally and theoretically. It is shown that the broadening is due to elastic phonon scattering by the composition fluctuations. A theoretical approach is used where the statistical and dynamical aspects of the phonon scattering are treated separately. The type, size, and number of the fluctuations responsible for the phonon line broadening are estimated. The theory is qualitatively consistent with the observed composition dependences.

DOI: 10.1103/PhysRevB.65.125203 PACS number(s): 78.30.Ly, 63.20.−e, 61.72.Bb

I. INTRODUCTION

The interest in isoelectronic alloys stems from the possibility to change their basic physical properties over a wide range by intentionally varying the alloy compositions. The distinguishing feature of alloys is a disorder in atomic distributions over lattice sites, producing properties of electron states and lattice dynamics. Wide-gap $Al_xGa_{1-x}N$ alloys are widely used for the fabrication of optoelectronic devices operating in the blue and violet regions of the spectrum.[1] However, despite significant progress in the preparation of these materials, achieved in recent years, many of their basic characteristics still remain poorly studied. This is particularly true for the phonon spectrum.

Vibrational spectra of alloys were studied in many theoretical papers, where a variety of approaches and models were developed. The coherent potential approach[2,3] uses the idea that the spectrum of a disordered system can be classified in terms of the quantum states that characterize the regular crystals. The phenomenological random element isodisplacement (REI) and modified REI (MREI)[4–6] methods were developed to describe the lattice dynamics of alloys. According to the REI and MREI models, ternary alloys are divided into two main classes (one- and two-mode classes), depending on the behavior of optical phonons at the Γ point.

The lattice dynamics of hexagonal $Al_xGa_{1-x}N$ alloys was studied theoretically and experimentally in Refs. 7–16. The one-mode behaviors of A_1(LO) and E_1(LO) phonons, predicted by different theoretical models, were found to agree well with experimental data. The behaviors of A_1(TO), E_1(TO), and E_2(high) phonons are more complicated because of mixing and crossing effects in some composition ranges, and the agreement between experimental and theoretical data is rather poor. The nonpolar E_2(low) phonon mode was not discussed at all in the literature. Information about the silent B_1(high) and B_1(low) modes, which are forbidden in Raman and IR spectra, is very scarce. The energy of the silent B_1(high) mode was reported in Ref. 12, where a weak dip in the continuum Raman spectrum in the frequency interval between longitudinal and transverse optical phonons was identified with the position of this mode. However, the calculated positions of the B_1(high) mode in Refs. 9 and 10 differ considerably from the data given in Ref. 12. Thus only observations of long-wave lattice vibrations and calculations of spectral DOS at the zero wave-vector have been reported so far.

To our knowledge, no data on second-order Raman scattering in $Al_xGa_{1-x}N$ were published. Second-order Raman spectra are of particular interest because they are formed by phonons with arbitrary wave vectors, and provide information about the phonon density-of-states (DOS) function which can be used as a test for lattice dynamics calculations.

An inherent feature of alloys is the composition fluctuations, which play an important role in their physical properties.[17] The phonon lines of alloys are inhomogeneously broadened due to composition fluctuations, in con-

trast to the phonon lines of regular crystals. Phonon line broadening was considered within the framework of perturbation theory[18–20] and the coherent potential approach[2,3] using the so-called single-site fluctuation approximation. The investigation of this effect provides valuable information about alloys, because it can answer the question of whether the atom distribution over the lattice sites is governed by a statistics law or not. Therefore, the composition dependence of the phonon line broadening can be an indicator of the degree of randomness of the alloy.

Data on the phonon line broadening in $Al_xGa_{1-x}N$ crystals are rather scarce. Experimental data on broadening of some of the optical modes were reported in Refs. 11 and 12. Theoretically, the disorder-induced broadening of the E_2(high) mode was considered in Ref. 21 using the spatial correlation model.

In this paper we describe studies of first- and second-order Raman scattering in $Al_xGa_{1-x}N$ alloys over the entire composition range. The composition dependence of the frequencies of all phonon modes active in the Raman scattering, including the nonpolar E_2(low) phonon mode, is traced in detail. A comparative analysis of the first- and second-order Raman spectra is used to obtain data about the phonon DOS and energy position of the B_1(high) silent mode in $Al_xGa_{1-x}N$ alloys.

Another subject of our experimental and theoretical studies is the influence of fluctuations on the phonon spectrum of alloys. Our theoretical approach assumes that the concept of phonons characterized by a wave vector is appropriate for a consideration of the vibrational motion of the system in the zero approximation, and that the elastic phonon scattering can account for the composition-dependent part of the Raman line broadening.

This paper is organized as follows. In Sec. II, the experimental procedure and the samples used in the experiments are described. In Sec. III, we present experimental results of the first-order Raman scattering, and discuss the obtained composition dependences of the optical phonon frequencies. An analysis of the second-order Raman spectra is also presented. In Sec. IV, a theoretical approach to the phonon line broadening caused by fluctuations is formulated. Experimental data are presented and analyzed within the framework of the developed theory.

Section V contains a summary. Preliminary results of our study of the composition dependence of optical phonon energies in hexagonal $Al_xGa_{1-x}N$ alloys were described elsewhere.[22]

II. SAMPLES AND EXPERIMENTAL PROCEDURE

We used a large set of $Al_xGa_{1-x}N$ samples with a difference in Al content of not more than 3–5 % in the entire composition range. 0.5-μm-thick $Al_xGa_{1-x}N$ epilayers in composition range of $0<x<0.5$ were grown on thin GaN buffer layers deposited on the *c*-plane sapphire in a Riber 32 molecular-beam epitaxy system.[23] 2–4-μm-thick $Al_xGa_{1-x}N$ epilayers with $0<x<0.5$ were grown by reduced-pressure metal-organic chemical vapor deposition on sapphire substrates, using low-temperature $Al_xGa_{1-x}N$ nucleation layers.[24] 1–4-μm-thick layers of $Al_xGa_{1-x}N$ alloys in a composition range of $0.5<x<1$ were grown by hydride vapor phase epitaxy on (111) silicon substrates without buffer layers.[25] The structural quality of the layers and the alloy composition were controlled by x-ray diffraction and electron probe microanalysis (EPMA). According to the x-ray data, all samples were single-crystal layers with a hexagonal modification without any polycrystalline inclusions or phase separation. The details of the x-ray measurements can be found in Ref. 16.

TABLE I. Raman selection rules for optical phonons in wurtzite-type crystals.

Scattering configuration	Allowed modes
$z(yy)\bar{z}$	E_2, A_1(LO)
$z(xy)\bar{z}$	E_2
$y(zz)\bar{y}$	A_1(TO)
$y(xz)\bar{y}$	E_1(TO)
$y(xx)\bar{y}$	E_2, A_1(TO)
$y(zy)x$	E_1(TO), E_1(LO)

Raman spectra of the $Al_xGa_{1-x}N$ layers were measured in a backscattering and 90° configuration at room temperature and at 100 K. Owing to the use of a large number of scattering geometries (Table I), we were able to avoid ambiguity in assigning the observed features in the spectra to phonons of a definite type of symmetry. The scattering geometries used in the experiment are given in Porto's notations of $y(zy)x$ type. Here the *z* direction is parallel to the optical *c* axis, and *x* and *y* are mutually orthogonal and oriented in an arbitrary manner in the substrate plane. An Ar^+ laser ($\lambda=488$ nm) was used as an excitation source. The spectral resolution was 1 cm^{-1}. Frequencies and the full width at half maximum (FWHM) of the phonon modes were determined by fitting Lorentzian line shapes to the measured Raman lines.

To exclude possible errors in measuring phonon frequencies caused by the effect of strain in $Al_xGa_{1-x}N$ layers, we studied alloys with the same composition but different layer thicknesses. It was found that layers with a thickness of more than 4 μ were nearly strainless. In addition, strain relaxation near the sample cleavage was observed even for thinner samples. Note that the geometries of scattering from the cleavage were used to detect the majority of Raman-allowed optical phonons (see Table I). As a result, we obtained composition dependences of phonon frequencies for nearly strainless $Al_xGa_{1-x}N$ samples. The effect of strain in $Al_xGa_{1-x}N$ alloys will be discussed in more detail in a separate paper.

III. EXPERIMENTAL RESULTS

A. Phonons in wurtzite structure

Hexagonal GaN, AlN, and $Al_xGa_{1-x}N$ alloys crystallize in a wurtzite structure [the C_{6v}^4 ($P6_3mc$) space group]. According to a factor group analysis at the Γ point, phonon modes in a hexagonal crystal belong to the irreducible representations

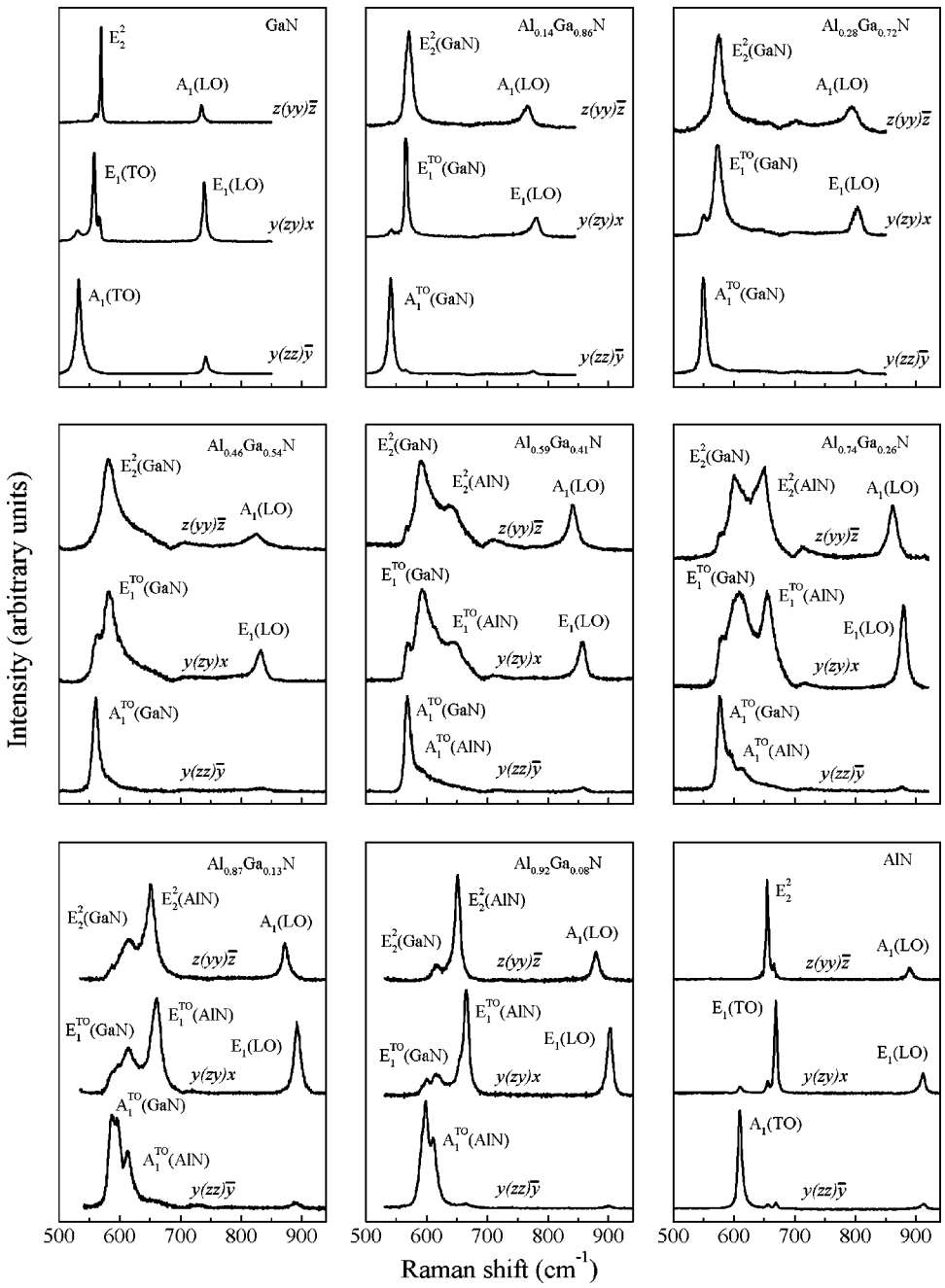

FIG. 1. Room-temperature polarized Raman spectra for GaN and AlN, and $Al_xGa_{1-x}N$ alloys.

$$\Gamma_{ac}+\Gamma_{opt}=(A_1+E_1)+(A_1+2B_1+E_1+2E_2).$$

Among optical phonons, the A_1 and E_1 modes are both Raman and IR active, the E_2 modes are only Raman active, and the B_1 modes are silent.[26] There are six optical modes A_1(TO), A_1(LO), E_1(TO), E_1(LO), E_2(high), and E_2(low) active in the first-order Raman scattering. The Γ-point phonon frequencies were well studied both for GaN and AlN.[27–31] Figure 1 shows polarized Raman spectra of GaN and AlN, and $Al_xGa_{1-x}N$ alloys with different compositions. For the Ga-rich region, the measured first-order polarized Raman spectra were found to be consistent with the selection rules for the wurtzite structure. However, the mode behavior in the Al-rich composition range is more complicated. Here we describe results which allow us to obtain a complete and self-consistent picture of the behavior of phonon modes in $Al_xGa_{1-x}N$ alloys.

B. A_1(LO) and E_1(LO) modes

It was found earlier in Refs. 11 and 12 that the frequencies of A_1(LO) and E_1(LO) modes in $Al_xGa_{1-x}N$ alloys shift toward higher energies with increasing Al concentration. However, the presence of free carriers in epilayers can result in an additional high-frequency shift of LO-phonon lines due to the formation of mixed plasmon–LO-phonon modes.[32,33] To exclude this effect, samples with low carrier concentrations were investigated. Hall measurements show electron concentrations in the range 10^{16}–10^{17} cm^{-3} for our samples.

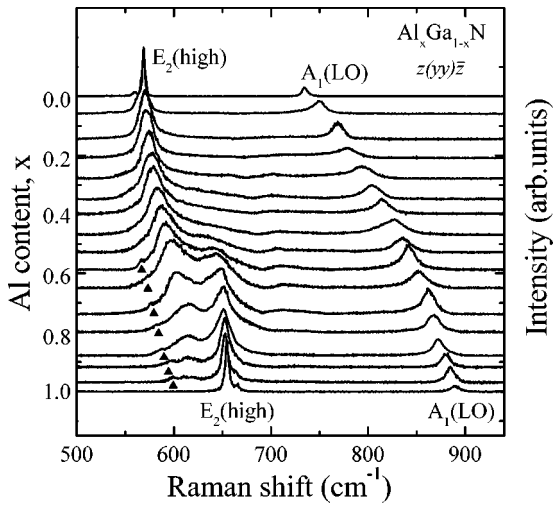

FIG. 2. Room-temperature Raman spectra for $Al_xGa_{1-x}N$ alloys obtained in a geometry corresponding to the E_2(high) and A_1(LO) phonon modes. The full triangles show positions of the A_1(TO) phonon line forbidden in this scattering geometry.

Note that the observation of the E_1(LO) mode is forbidden in backscattering geometry, in contrast to the A_1(LO) mode. To make the assignment more reliable, we used a 90° scattering geometry in which the E_1(LO) phonon mode is allowed according to the selection rules (Table I).

The experimental data obtained for A_1(LO) and E_1(LO) modes are shown in Figs. 2 and 3, respectively, and positions of these modes as a function of Al content for $0<x<1$ are presented in Fig. 4(a). It is clear that in the entire composition range each LO mode manifests itself as a single line, and the separation between the lines grows monotonically with increasing Al concentration. This observation is consistent with the fact that the E_1(LO)-A_1(LO) separation for AlN is larger than that for GaN.

Note that our results differ from the data of Ref. 12 where the frequencies of the A_1(LO) and E_1(LO) phonons coincided within an interval of $0.5<x<0.7$. In our opinion, this could be due to a relaxation of selection rules in the samples with $x>0.5$ used in Ref. 12. As an illustration, Fig. 5 shows Raman spectra obtained for two samples having the same Al content, but exhibiting different structural perfections. It is seen that for a sample with a poorer crystal structure, a single broad line rather than two [A_1(LO) and E_1(LO)] modes is detected in the scattering geometries used.

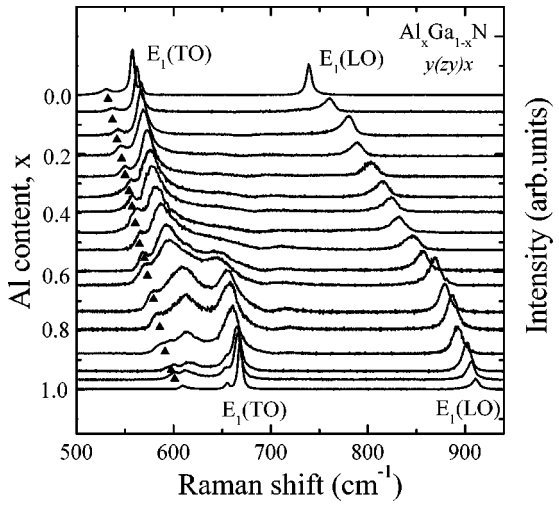

FIG. 3. Room-temperature Raman spectra for $Al_xGa_{1-x}N$ alloys obtained in a geometry corresponding to E_1(TO) and E_1(LO) phonon modes. The full triangles show positions of the A_1(TO) phonon line forbidden in this scattering geometry.

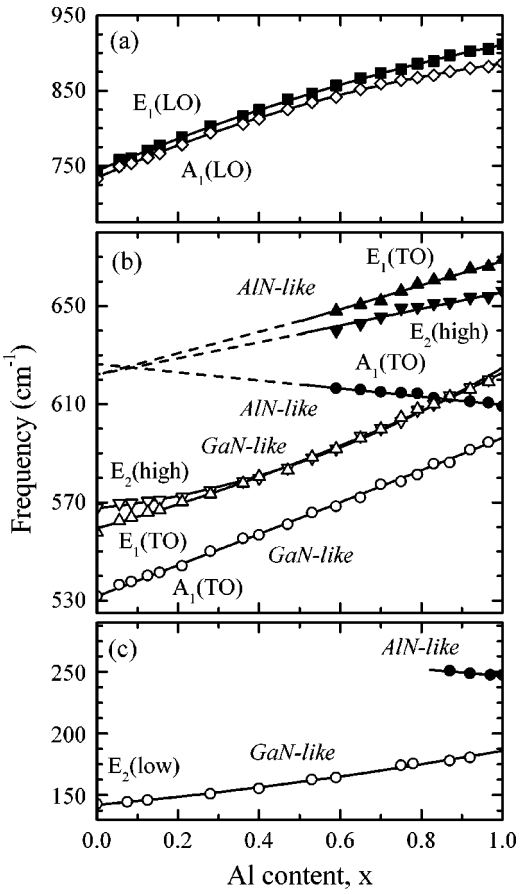

FIG. 4. Frequencies of optical modes vs $Al_xGa_{1-x}N$ alloy composition. Top panel: E_1(LO) (squares) and A_1(LO) (diamonds). Middle panel: A_1(TO) (circles), E_1(TO) (triangles), E_2(high) (inverted triangles); open circles, triangles, and inverted triangles are for GaN-like modes, and full circles, triangles, and inverted triangles are for AlN-like modes. Bottom panel: E_2(low) (open symbols) correspond to GaN-like modes, and full symbols correspond to AlN-like modes.

Our results for A_1(LO) phonons also revealed a discrepancy with the data of Ref. 11 for $0<x<0.6$. A_1(LO) phonons were detected in Ref. 11 at higher frequencies compared with our data for $Al_xGa_{1-x}N$ alloys with an identical Al content. It can be supposed that this discrepancy could be caused by a higher concentration of free carriers in the samples used in Ref. 11.

No extra lines were found for $Al_xGa_{1-x}N$ alloys in the frequency range of LO phonons. Thus our findings clearly confirm the theoretical predictions of the one-mode type behavior of longitudinal phonons.[7,9,12] The one-mode behavior of LO phonons and the high sensitivity to the Al content (the frequency of each LO phonon changes by about 160 cm^{-1}

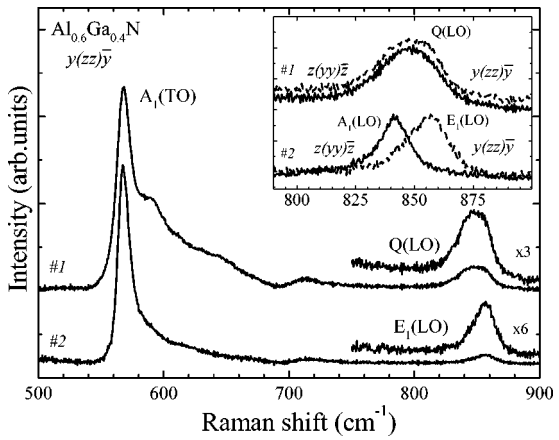

FIG. 5. Raman spectra for two samples having the same Al content, but exhibiting different structural perfections. The inset shows that for a sample with a poorer crystal structure, a single broad line, rather than two [A_1(LO) and E_1(LO)] modes, is detected in the scattering geometries used.

from GaN to AlN) are suitable for estimating the Al content in $Al_xGa_{1-x}N$ alloys. Positions of A_1(LO) and E_1(LO) phonons as functions of the Al content can be approximated by equations taking into account a slight bowing of the curves:

$$A_1(\mathrm{LO}) = 734 + 153x - b_{A_1(LO)}x(1-x) \tag{1}$$

and

$$E_1(\mathrm{LO}) = 742 + 170x - b_{E_1(LO)}x(1-x), \tag{2}$$

with negative bowing parameters $b_{A_1(LO)} = -75\ \mathrm{cm}^{-1}$ and $b_{E_1(LO)} = -65\ \mathrm{cm}^{-1}$.

C. E_2(high) and E_1(TO) modes

In the composition range $0<x<0.28$, E_2(high) and E_1(TO) modes have appreciably differing frequencies, and each phonon is detected as a single line in a relevant scattering geometry (Figs. 2 and 3). However, starting from $x=0.28$, a mixing of these modes occurs and, as a consequence, the spectra in the scattering configurations corresponding to E_2(high) and E_1(TO) phonons have identical shapes. As a consequence, it is impossible to distinguish one phonon from the other within the interval $0.28<x<0.7$. In addition, for $x>0.36$, a shoulder in the line appears at a higher frequency. Its intensity grows with increasing Al content, while the intensity of the lower-frequency peak decreases. In the interval $0.7<x<1$, the higher frequency peak narrows, and is again detected at different frequencies for E_2(high) and E_1(TO) modes in corresponding scattering geometries. The lower frequency peak has the same shape and position for both scattering configurations. Thus it can be stated that the presence of two lines in polarized Raman spectra corresponding to E_2(high) and E_1(TO) phonons is an inherent property of these modes for $0.36<x<1$.

The behavior of the E_2(high) phonon described above was earlier observed in Refs. 11 and 12. The authors described their experimental results in terms of the two-mode behavior of the E_2(high) phonon. Our findings agree with their interpretation. In our studies, we succeeded in tracing the behavior of this phonon mode in the range of very high Al contents. At extremely high Al concentrations ($x \approx 0.98$), a narrowing of the GaN-like E_2(high) phonon line was found to take place. This points to a preferentially localized nature of this vibration. Positions of the E_2(high) mode versus Al content for $0<x<1$ are presented in Fig. 4(b).

Let us return to the E_1(TO) phonon mode. The theoretical considerations presented in Refs. 9 and 10 predicted a two-mode behavior of this phonon. The experimental evidence of such a behavior was found in IR reflection and IR ellipsometry spectra in Refs. 13 and 14. However, no reliable Raman data pointing to a two-mode behavior of E_1(TO) phonons was available so far. The pattern of transformation of Raman spectra revealed in our experiments (Fig. 3) provides a convincing proof of the two-mode behavior of the E_1(TO) phonon. Positions of the E_1(TO) mode as a function of Al content for $0<x<1$ are presented in Fig. 4(b).

Our data for the GaN-like E_1(TO) mode are in fairly good agreement with the IR reflection and IR ellipsometry data given in Refs. 13 and 14; however, the results for the AlN-like E_1(TO) mode differ considerably. In our opinion, this discrepancy can be caused by several factors. First, the set of $Al_xGa_{1-x}N$ samples used in Refs. 13 and 14 was small, and the difference in Al contents was very large (more than 25%). In our experiments, a much larger set of samples was employed to obtain information about the Al-like E_1(TO) mode. Second, Raman spectroscopy is a direct technique for the observation of optical phonons because phonons manifest themselves in the Raman spectra as separate lines. In IR spectroscopy, a fitting procedure is needed to deduce the data on phonon frequencies. As a consequence, the accuracy of the determination of the phonon position depends on fitting parameters and the procedure used.

D. Mode of the A_1(TO) symmetry

Figure 6 depicts the transformation of the Raman spectrum depending on Al content in the scattering configuration corresponding to the A_1(TO) phonon mode. We found that this mode manifests itself in a Ga-rich composition range as a single line which experiences a high-frequency shift with increasing Al content, and whose FWHM remains nearly the same in a wide composition range of $0<x<0.4$. These data are consistent with other works.[11,12]

At high Al contents, this line exhibits an asymmetric broadening toward higher frequencies, the low-frequency edge remaining as sharp as before. In addition, two features appear at the high-frequency edge of this band. They change their positions and shapes as the alloy composition is varied. As evidenced by our polarization measurements (Fig. 1), these features cannot be interpreted as resulting from the modes of other symmetries. It was also found that intensities of the most low- and high-frequency peaks in this scattering configuration are proportional to the Ga and Al contents, respectively. The relative intensity of the third feature occupying the position between the peaks discussed above has a

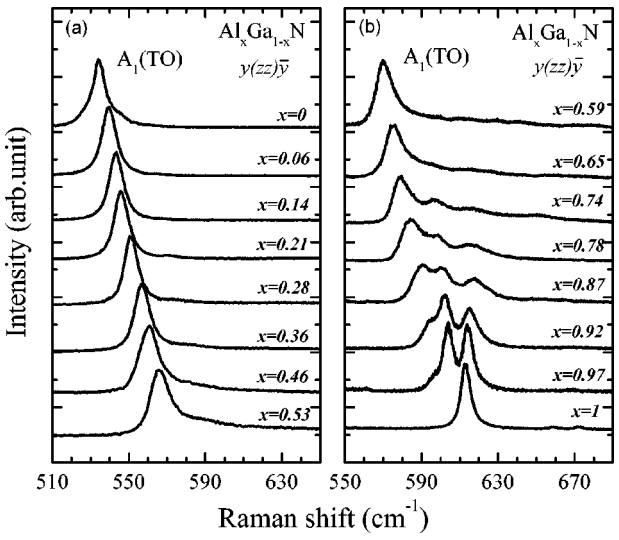

FIG. 6. Raman spectra at 100 K obtained in a geometry corresponding to the A_1(TO) phonon mode for $Al_xGa_{1-x}N$ alloys.

weak dependence on Al content within a composition interval of $0.87<x<1$, where all three lines are well resolved.

The spectrum transformation described above can be understood if we assume that two lines having the opposite dependences of intensities on the Al content are GaN- and AlN-like phonon modes of A_1(TO) symmetry. This conclusion is consistent with the theoretical predictions of the two-mode behavior of A_1(TO) phonon given in Refs. 8 and 10. The positions of GaN- and AlN-like A_1(TO) modes as a function of Al content for $0<x<1$ are presented in Fig. 4(b). The dependence of the GaN-like A_1(TO) phonon mode on the Al content can be approximated by the equation

$$A_1(\mathrm{TO}) = 531.8 + 64.5x - b_{A_1(TO)}x(1-x), \qquad (3)$$

with small positive $b_{A_1(TO)} = 1.9\ \mathrm{cm}^{-1}$. Due to a nearly linear behavior and a high sensitivity to the Al content, this approximation can be efficiently used for an estimation of Al content in hexagonal $Al_xGa_{1-x}N$. A more detailed description of the A_1(TO) phonon mode transformation in Al-rich alloys, together with a theoretical approach which describes changes in the vibration spectrum at a sufficiently strong perturbation resulting from the isoelectron substitution, was given elsewhere.[16]

E. Mode of the E_2(low) symmetry

The experimental data obtained for the E_2(low) mode are shown in Fig. 7. At low Al contents, this phonon is detected as a single peak. With increasing Al content, the phonon line shifts toward higher frequencies and experiences a strong broadening. At high Al contents $x>0.6$, a feature appears in the spectrum at higher frequencies. It changes its position and intensity as the alloy composition is varied. A careful analysis has shown that this feature in the spectrum represents an intrinsic first-order scattering, and is not associated with disorder-activated acoustic DOS's.

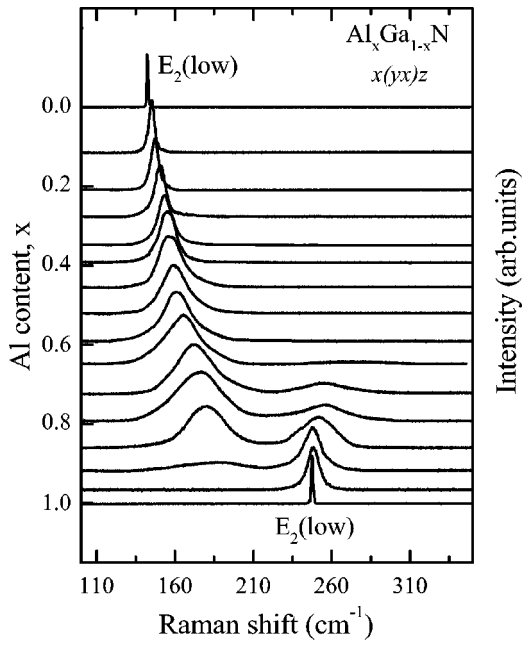

FIG. 7. Raman spectra for $Al_xGa_{1-x}N$ alloys obtained in a geometry corresponding to the E_2(low) phonon mode.

It was found that the intensity of the low-frequency line in the spectrum becomes less intense with increasing Al content. In the limit of very high Al concentrations, it is a weak peak, with a maximum at 190 cm^{-1}. The intensity of the high-frequency line grows with increasing Al content. It narrows and shifts toward lower frequencies, and in the limit $x\to 1$ tends toward the position typical of the E_2(low) phonon in AlN. For pure AlN, only a single line at 249 cm^{-1}, corresponding to the E_2(low) phonon, is detected in the spectrum.

The pattern described above can be understood in terms of a two-mode behavior of the E_2(low) phonon. We assume that two lines whose intensities are proportional to the content of two basic components of the alloy are the GaN- and AlN-like phonon modes of E_2(low) symmetry. The positions of these modes versus Al content for $0<x<1$ are presented in Fig. 4(c). The dependence of the GaN-like E_2(low) mode on the Al content can be approximated by

$$E_2(\mathrm{low}) = 142.8 + 43.5x - b_{E_2(low)}x(1-x), \qquad (4)$$

with the positive bowing parameter $b_{E_2(low)} = 14.5\ \mathrm{cm}^{-1}$.

We have found only one paper concerning E_2(low) phonon in $Al_xGa_{1-x}N$ alloys.[11] It gives data for an alloy with $x=0.36$, where this phonon was detected as a broad line centered at 152 cm^{-1}. We obtained the position of the E_2(low) line at 154 cm^{-1} for $x=0.36$, which is consistent with the data of Ref. 11.

Recently a paper appeared that was concerned with Fourier transform infrared reflectance and Raman measurements of the composition dependence of energies of five optical phonons in $Al_xGa_{1-x}N$ alloys. For the Al content $0<x<0.8$, the composition dependences for A_1(TO), E_1(TO), E_2(high), and A_1(LO) phonons, given in Ref. 34 are quali-

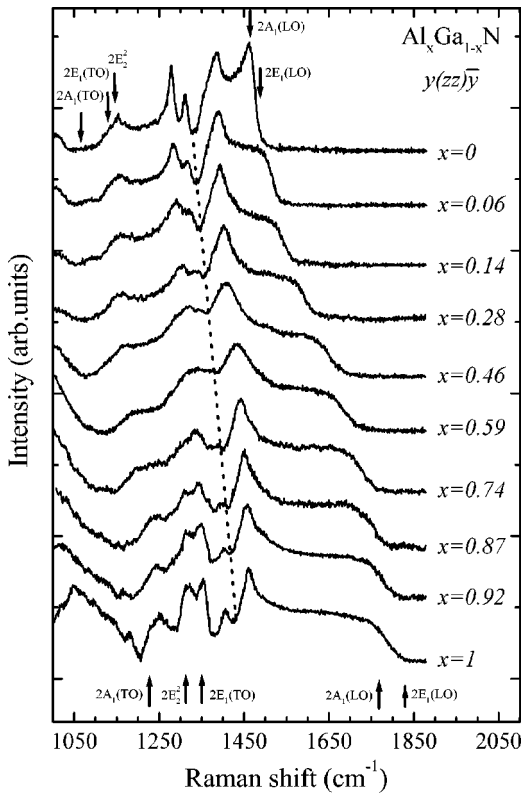

FIG. 8. Room-temperature second-order spectra for GaN and AlN, and $Al_xGa_{1-x}N$ alloys in the range of overtones of optical phonons. The arrows show the positions of overtones of zone-center phonons for GaN (top) and AlN (bottom) lying in this spectral region.

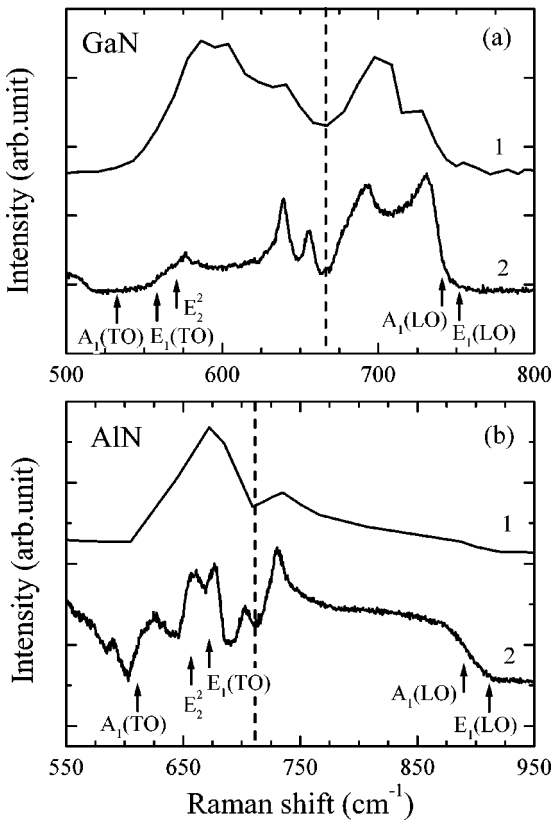

FIG. 9. Experimental phonon DOS obtained from neutron experiments in Refs. 35 and 36 for GaN (top panel, curve 1) and AlN (bottom panel, curve 1), and second-order Raman spectra for GaN (top panel, curve 2) and AlN (bottom panel, curve 2), plotted by scaling the frequency axis by a factor of 1/2. The arrows show the positions of overtones of zone-center phonons for GaN (top) and AlN (bottom) lying in this spectral region.

tatively similar to those shown in Fig. 4 of our paper. However, the dependences exhibit a low-energy shift for all the phonons compared with our data for the same compositions. This difference can be explained by the fact that, as stated by the authors of Ref. 34, their samples had a strong tensile in-plane strain, while our samples were nearly strainless. Unfortunately, the data for the Al content within the range $0.8 < x < 1$, which is of particular interest, were not given in Ref. 34.

F. Second-order Raman scattering and B_1(high)-symmetry silent mode

1. Second-order Raman spectrum

We managed to measure the second-order polarized Raman spectra of $Al_xGa_{1-x}N$ alloys for $0 < x < 1$. Figure 8 shows room-temperature second-order spectra in the range of overtones, and a combination of optical phonons for the entire composition range, from GaN to AlN. It is known that features of the two-phonon spectra are determined by the singularities in the phonon DOS function closely associated with flat regions of phonon dispersion curves. In Fig. 9 we compare our second-order Raman spectra for GaN and AlN plotted by scaling the frequency axis by a factor of 1/2 (the overtone approximation) and the experimental DOS obtained from neutron experiments.[35,36] It can be seen that basic features of the second-order spectra correlate well with singularities in the experimental DOS. Of particular interest is an excellent correlation between the gap separating the dispersion regions of transverse and longitudinal optical phonons in the phonon DOS and the corresponding minimum in second-order Raman spectra.

It is clearly seen in Fig. 8 that, for all alloys, a distinct minimum similar to the minimum in the second-order Raman spectra of GaN and AlN is present. This suggests that dispersion regions of TO and LO phonons are separated for all compositions of $Al_xGa_{1-x}N$. Figure 8 also shows the positions of overtones of the Γ-point optical phonons, from which it is evident that the dispersion region of LO phonons becomes wider and the dispersion region of TO phonons becomes narrower with increasing Al content.

Another distinctive feature of all the second-order spectra of alloys shown in Fig. 8 is a sharp maximum in the region of 1300–1340 cm^{-1}. It can be seen that the position of this maximum depends only slightly on the Al content. As is apparent from Fig. 9, similar maxima in second-order spectra of GaN and AlN correlate well with singularities in the phonon DOS's that lie near 695 and 725 cm^{-1}, respectively. As noted above, no data on the phonon DOS of $Al_xGa_{1-x}N$ are available; however, it can be supposed that a similar corre-

lation between the maxima in second-order spectra and phonon DOS is valid for alloys. In this case the phonon DOS of $Al_xGa_{1-x}N$ alloys must have a corresponding singularity within the range 695–725 cm^{-1}. Below, we try to understand the origin of this singularity.

2. Silent B_1(high) mode

Optical phonons of B_1 symmetry in crystals of the C_{6v}^4 $[(P6_3mc)]$ space group are silent i.e., both B_1(low) and B_1(high) modes are forbidden in Raman and IR spectra.[26] There have been numerous theoretical calculations of the position of these modes in AlN and GaN,[37–42] but only the authors of Refs. 38 and 42 succeeded in measuring B_1 modes in these compounds by inelastic x-ray scattering. In Ref. 12, a weak dip in the first-order Raman scattering was observed for hexagonal $Al_xGa_{1-x}N$ alloys in the spectral region between longitudinal and transverse optical phonons. Its Raman shift increases linearly with Al content. The hypothesis was put forward that this feature suggests an interference between a discrete B_1(high) silent mode and the continuum of excitations caused by q-dependent processes in alloys. As a result, the energy of the silent B_1(high) mode was identified with the position of this dip. However, lattice dynamics calculations for hexagonal $Al_xGa_{1-x}N$ alloys, reported in Refs. 9 and 10 demonstrated that the B_1(high) mode position is 50–70 cm^{-1} higher than the dip position.

We tried to reveal the origin of the dip in the first-order spectrum by comparing its position with the features in the second-order spectra. Figure 10 presents first-order Raman spectra for some of $Al_xGa_{1-x}N$ alloys together with second-order spectra for these samples plotted by scaling the frequency axis by a factor of 1/2. In the first-order spectra of alloys shown with a magnification, a dip and a distinct maximum at the high-frequency edge of this dip are clearly seen. It is evident that the positions of the dip and the minimum in the second-order spectra discussed above correlate well. A good correlation is also seen between the maximum in the first-order spectra and a corresponding sharp maximum in the second-order spectra. We have found that both correlations hold for the entire composition range $0<x<1$.

Compared with GaN and AlN, $Al_xGa_{1-x}N$ alloys exhibit a lower structural quality and, therefore, a disorder-activated phonon DOS can manifest itself in first-order spectra. In our opinion, the dip in the first-order Raman scattering of the $Al_xGa_{1-x}N$ alloys results from the gap in the phonon DOS between the dispersion regions of TO and LO optical phonons. The maximum at the high-energy edge of this dip is also attributable to q-dependent processes, and results from the singularity in the phonon DOS of $Al_xGa_{1-x}N$ alloys at 697–725 cm^{-1}. This conclusion is supported by the absence of a dip and a maximum in first-order Raman scattering of perfect GaN and AlN crystals shown in Fig. 10.

As shown in Refs. 10, 38, 42, and 43, the dispersion branches of the B_1(high) phonon modes of GaN and AlN occupy a narrow energy range along high-symmetry directions in the Brillouin zone. This can result in a strong singularity associated with this mode in phonon DOS. According to theoretical calculations performed in Refs. 9 and 10 for

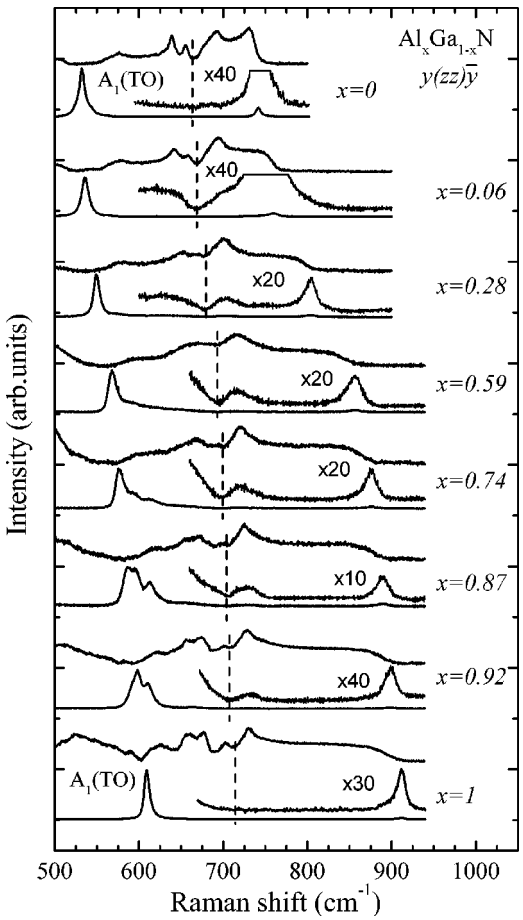

FIG. 10. Room-temperature first-order Raman spectra for $Al_xGa_{1-x}N$ $(0<x<1)$ in a geometry corresponding to the A_1(TO) phonon mode and second-order Raman spectra for alloys plotted by scaling the frequency axis by a factor of 1/2.

$Al_xGa_{1-x}N$ alloys, a distinctive feature of the B_1(high) phonon mode is a weak dependence of its position on Al content. Just this dependence is typical of the behavior of the singularity at 697–725 cm^{-1} in the phonon DOS of $Al_xGa_{1-x}N$ alloys.

Figure 11 shows the position of the maximum under discussion in the first-order spectra as a function of the Al content. This figure also shows the calculated dependences of the position of the B_1(high) mode taken from Refs. 9 and 10 and experimental data for AlN and GaN from Refs. 38 and 42. It can be seen that our data are in good agreement with both calculations and experiment for Ga-rich alloys. This indicates that the energy of the silent B_1(high) mode in $Al_xGa_{1-x}N$ alloys can be identified with the position of the maximum in the first-order spectra at 695–725 cm^{-1}, rather than the dip position. At the same time, in the Al-rich region, our data differ from theory and experiment. The difference between our data and inelastic x-ray scattering data for AlN (Ref. 38) can be explained by the fact that the maximum in the phonon DOS associated with the B_1 mode does not correspond to the Γ point. Indeed, as seen from Fig. 2 of Ref. 38, the dispersion curves along the Γ-K-M and Γ-M directions, which most probably form this maximum in phonon DOS's, are situated lower in energy than that in the Γ point.

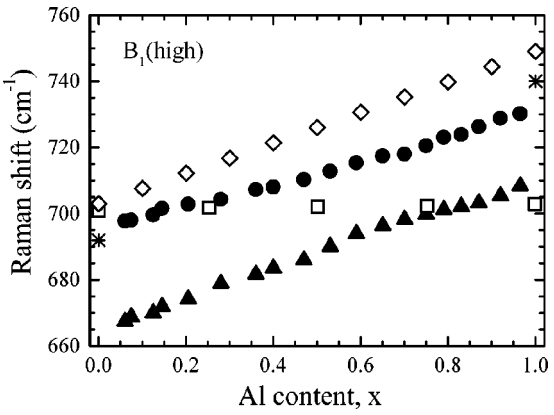

FIG. 11. Positions of the dip (full triangles) and the maximum that can be ascribed to B_1(high) silent mode (full circles) as a function of Al content. The asterisks show the experimental data taken from Refs. 38 and 42. *Ab initio* calculations of the position of B_1(high) mode, taken from Ref. 9 (open diamonds) and Ref. 10 (open squares), are also shown.

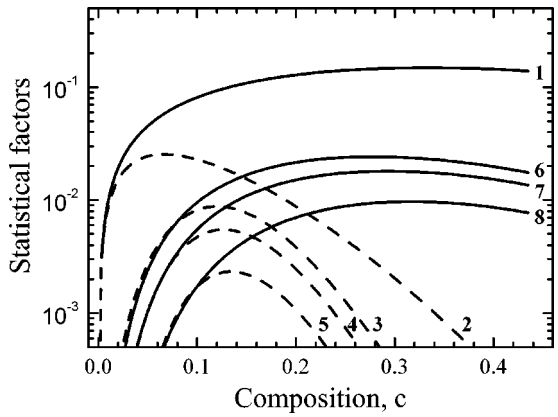

FIG. 12. Statistical factors of the scattering process calculated in different approximations. Curve 1 is the factor of the single-site approximation $\mathcal{F}_1[c,(1-c)]=c(1-c)^2$. Curve 2 is the cluster statistical factor $\mathcal{F}_{n_s}[c,(1-c)]$ of Eq. (6) for the single-site cluster $s=1$. Curves 3, 4, and 5 are the cluster statistical factors defined by $\Sigma_{s\geqslant s_0}\mathcal{F}_{n_s}[c,(1-c)]$ for $s_0=3$, 4, and 6, respectively. Curves 6, 7, and 8 are the statistical factors $\mathcal{F}_{n,\bar{p}}[c,(1-c)]$ as given by Eq. (9) for $n=15$, 20, and 30 at $\bar{p}=0.255$, 0.235, and 0.215, respectively.

The discrepancy of our data with theoretical calculations for Al-rich alloys can be resolved with future lattice dynamics calculations and additional inelastic x-ray-scattering measurements.

IV. COMPOSITION DEPENDENCE OF THE FIRST-ORDER PHONON LINE BROADENING IN ALLOYS

Regular crystals are characterized by a long-range order which restricts the first-order Raman spectrum to phonons having small wave vectors equal to the difference between the wave vectors of incident and scattered photons. This wave-vector conservation law is violated in alloys which are systems with broken long-range order, and quantitative data on this violation are important characteristics of the alloy itself.

There are two mechanisms for this conservation law breaking. The first is concerned with electron motion in the alloy. The localization of electrons (or holes), or their scattering by the fluctuation potential of a disordered medium, gives rise to a violation of the wave-vector conservation law in Raman scattering if the disturbed electron states play the role of intermediate states in the Raman process. This is highly probable for resonant Raman scattering at excitation near the band edge. The second mechanism of wave-vector conservation law breaking, which is due to specific features of the lattice dynamics of disordered systems, can be more important for the Raman process if the incident photon energy is far away from the resonance. This mechanism is an elastic scattering of phonons by composition fluctuations.

The efficiency of the first-order Raman scattering is defined by corresponding Raman polarizability[44] which is linear in atomic displacements. The shape of the phonon Raman line of a branch j, as a function of frequency ω which defines the Raman shift of the scattered photon energy at a phonon wave-vector equal to the difference between the wave vectors of incident and scattered photons $\mathbf{q}=\mathbf{k}-\mathbf{k}'$, can be presented for the Stokes process at zero temperature as

$$I(\mathbf{q},\omega)=\frac{1}{\pi}\mathrm{Im}\frac{1}{\omega^2-\omega^2(j\mathbf{q})+t_{jj\mathbf{q},\mathbf{q}}(\omega)}. \quad (5)$$

Here t is the complex scattering matrix which can be written as $t_{jj\mathbf{q},\mathbf{q}}(\omega)=\Delta_{j\mathbf{q}}(\omega)-i\gamma_{j\mathbf{q}}(\omega)$.

The multiple-scattering approach[2,3] to the calculation of the scattering matrix and phonon Green's function is used if the scattering process can be considered as a sequence of independent scattering events. For a crystal with substitution defects, the calculation procedure was developed in Refs. 18–20, 45, and 46 The broadening can be presented as

$$\gamma_{j\mathbf{k}-\mathbf{k}'}(\omega)=\{\mathcal{F}_1[c,(1-c)]G^A+\mathcal{F}_1[(1-c),c]G^B\}, \quad (6)$$

where $\mathcal{F}_1[x,y]$ are the statistical factors, x and y are the concentrations of atoms A and B constituting the solid solution, and functions $G^{A,B}$ are the weighted density of phonon states. In the single site approximation $G^{A,B}$ can be expressed through the single-site Green's, function of the ideal crystal,[19,20] and the statistical factors are equal to $\mathcal{F}_1[x,y]=xy^2$. Figure 12 shows the single-site function $\mathcal{F}_1[c,(1-c)]$, and gives a comparison with statistical multipliers of further approximations.

It follows from lattice percolation theory[47–50] that the concentration dependence of the correct number of spatially isolated single-site fluctuations differs significantly from that used in the simplified approach. This restricts the region of applicability of the single-site perturbation approach, and shows that it can be useful only in the limit of very low concentrations of scattering centers.

In order to improve the approach to the statistical problem, we consider scattering over the lattice clusters. The number of clusters at a given concentration can be found for the $Al_xGa_{1-x}N$ alloy by using the results available for the fcc lattice and neglecting, therefore, a small difference between the wurtzite and zinc blende lattices. The percolation

threshold occurs in the fcc sublattice at $c \approx 0.2$. The same is true for B atoms in the region of small values of $(1-c)$.

We assume that in this case the major role of factors occurring due to statistics will be preserved. Therefore, we reduce the solution of the problem of the composition dependence of the scattering efficiency to finding statistical factors which can be written as

$$\mathcal{F}_{n_s}[c,(1-c)] = n_s\{c,(1-c)\}(1-c)^2, \tag{7}$$

or as rapidly converging sums of such expressions, where $n_s\{c,(1-c)\}$ is the concentration n_s of the clusters consisting of s atoms A.[47–50]

Figure 12 demonstrates $\mathcal{F}_{n_1}[c,(1-c)]$ and some sums of $\mathcal{F}_{n_s}[c,(1-c)]$ for clusters of different sizes. A comparison of $\mathcal{F}_{n_1}[c,(1-c)]$, with a statistical multiplier $\mathcal{F}_1[c,(1-c)]$ of the single-site approximation, reveals a narrow range of concentrations where both approximations coincide and where, therefore, the single-site approximation is statistically acceptable.

The factor $\mathcal{F}_{n_1}[c,(1-c)]$ and sums of $\mathcal{F}_{n_s}[c,(1-c)]$ for $s \geqslant 3$, 4, and 6 in Fig. 12 demonstrate a rapid decrease in the number of clusters and the scattering efficiency, both with increases of the cluster size s and concentration c. Therefore, finite-size fluctuations of a more general character should be considered to describe the scattering in the entire composition range.

Above the percolation threshold almost all atoms of a given component of the alloy belong to the network of the percolation cluster.[47–50] The random distribution of atoms of two kinds over sublattice sites gives rise to the formation of regions where the concentration of the alloy deviates from the averaged value. The size of such a region and the magnitude of the deviation of the concentration, together with the amplitude of the perturbation caused by the extra atoms, define the phonon scattering efficiency in this case.

First of all, we have to find the probability of the composition fluctuation at a random filling of the volume consisting of n lattice sites by atoms of the first and second kinds, with average concentrations of c and $(1-c)$, respectively. The probability to find configurations with $n_{c+\bar{p}} = n(c+\bar{p})$ atoms of the first kind and $n_{1-c-\bar{p}} = n(1-c-\bar{p})$ atoms of the other kind is proportional to the binomial coefficient, and can be presented as

$$W^n_{n_{\bar{p}}} = \frac{n!}{n_{c+\bar{p}}!\, n_{1-c-\bar{p}}!} c^{n_{c+\bar{p}}} (1-c)^{n_{1-c-\bar{p}}}, \tag{8}$$

where the possible deviation $n_{\bar{p}} = n\bar{p}$ is restricted by the interval $-n_c \leqslant n_{\bar{p}} \leqslant n_{1-c}$. At sufficiently large n, the factorials n, $n_{c+\bar{p}}$, and $n_{1-c-\bar{p}}$ can be transformed into a continuum form with the help of the Stirling formula. As a result, for the composition dependence of the statistical factors we obtain

$$\mathcal{F}_{n,\bar{p}}[c,(1-c)] = \frac{(1-c)^2}{\sqrt{2\pi}} \left(\frac{c}{c+\bar{p}}\right)^{n(c+\bar{p})} \times \left(\frac{1-c}{1-c-\bar{p}}\right)^{n(1-c-\bar{p})}. \tag{9}$$

G_A and G_B are assumed to be analogous to the parameters introduced in Eq. (6). The function $\mathcal{F}_{n,\bar{p}}[(1-c)c]$ can be obtained from Eq. (9) by replacing the argument c by $(1-c)$, and vice versa.

Figure 12 presents functions $\mathcal{F}_{n,\bar{p}}[c,(1-c)]$ for $n = 15$, 20, and 30 at $\bar{p} \approx 0.2$. The last value was taken to be nearly equal to the percolation concentration over lattice sites for the fcc sublattice. This value makes possible the formation of a ''percolation'' cluster of finite size n by extra $n\bar{p}$ atoms. A comparison of functions $\mathcal{F}_{n,\bar{p}}[c,(1-c)]$ at $\bar{p} \approx 0.2$ with the cluster statistical factors shows that their full coincidence can be reached in the region of small $c \leqslant 0.10$ as a result of small variations of $n\bar{p}$. Functions $\mathcal{F}_{n,\bar{p}}[c,(1-c)]$ can be used to extrapolate the composition dependence of the scattering probability from the cluster region to the high concentration region.

The results of this section show that the composition dependence in the region of $c \leqslant 0.1$ is very sensitive to the size of fluctuations. A position of the maximum of the factor $\mathcal{F}_{n,\bar{p}}[c,(1-c)]$ also shifts with n, and can be informative about the fluctuation size. The results obtained allow us to assume that a regular composition dependence, asymmetrical with respect to $c = 0.5$, results from a random distribution of the alloy constituents.

A. Composition dependence of the linewidth of E_1(LO), A_1(LO), E_2(high), E_1(TO), and A_1(TO) phonon modes

The experimental data for $Al_xGa_{1-x}N$ alloys demonstrate a pronounced broadening of the phonon lines which depends on the alloys composition. Figure 13 shows the dependence of the linewidth of E_1(LO), A_1(LO), E_2(high), E_1(TO), and A_1(TO) phonon modes on aluminum content. In all the cases the experimentally measured broadening of the phonon lines has a background which, for given phonon lines, has different values at the limiting concentrations $x = 0$ and 1. The origin of this background can be attributed first of all to the anharmonic decay of a phonon state. Probably the scattering of the phonons by structural and chemical defects, as well as phonon interaction with free careers, can give detectable effects in some cases.

The composition dependence of the broadening of all the lines exhibits an asymmetry with respect to the point $x = 0.5$. The sign of the asymmetry is opposite for the pair of lines A_1(LO) and E_1(LO) as compared with lines A_1(TO) and E_1(TO). The A_1(TO) and E_1(TO) linewidths increase slowly at a low aluminum concentration, and reach a pronounced maximum at $x \approx 0.65$–0.7. The A_1(LO) and E_1(LO) linewidths increase much faster at a low aluminum concentration, and show a maximum at $x \approx 0.35$. On the

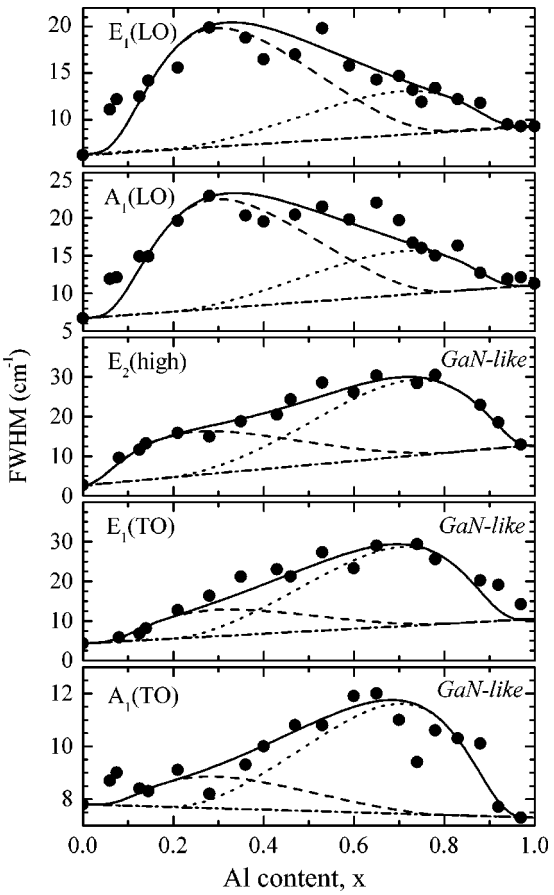

FIG. 13. Experimental and calculated composition dependences of the phonon line broadening. Full dots are the experimental dependences of FWHM's vs Al content in $Al_xGa_{1-x}N$ alloys for E_1(LO) and A_1(LO) phonons, and for GaN-like branches of E_2(high), E_1(TO), and A_1(TO) modes. The dashed line presents the composition dependence of $\mathcal{F}_{n,\bar{p}}[c,(1-c)]G_A$. The dash-dotted line is the dependence of $\mathcal{F}_{n,\bar{p}}[(1-c),c]G_B$, and the solid line is their sum.

other hand, the linewidth of the E_2(high) mode has a less asymmetrical composition dependence.

B. Fitting of the experimental data and discussion

Before fitting, the background of the phonon linewidth was subtracted. The values of the background for intermediate concentrations were obtained by means of a linear interpolation between the two limiting concentrations. The composition dependence of the remaining fraction of the broadening was fitted by means of the curves obtained by using Eq. (9), with a substitution of x for c.

The results for five phonon branches are presented in Fig. 13. A comparison of calculated curves with experimental data shows that there is a resonable agreement with the experimental points in the entire composition interval.

Despite a considerable difference in the absolute values of the broadening for five phonon bands in Fig. 13, we should note a similar behavior of the observed dependences. The experimental data show a pronounced asymmetry of a composition dependence with respect to $x=0.5$, and curves for E_1(LO) and A_1(LO) phonons resemble the mirror reflections of curves for E_1(TO) and A_1(TO) phonons. The calculated curves were obtained by the assumption that $G_A > G_B$ in the first case and $G_A < G_B$ in the second one.

It is also worth noting that the ratios G_A/G_B and G_B/G_A used to fit the experimental data have comparable values in all the cases considered. This fact can be attributed to the common nature of the perturbation of the phonon motion, namely, to the difference in masses of substituted and host atoms.

At the same time, the experimental points have a considerable spread as compared with smoothed theoretical curves. These deviations exceed the possible experimental errors and have a random character which, as can be supposed, reflects the differencies in the quality of the samples used in experiments. All of the theoretical dependences were obtained for randomly distributed atoms A and B, and any deviation from randomness can cause a corresponding change in the broadening resulting in the spread of the experimental points. All of the fitting curves were obtained for $n=30$ in Eq. (9). This corresponds to the linear size of the fluctuation approximately equal to three interatomic distances in the disordered sublattice. This value has to restrict the region of the wave vectors allowed in the Raman process by values satisfying the inequality $q \leqslant \pi/3a$, where a is the lattice constant. Taking into account the data on dispersion of the phonon branches, we can conclude that the observed broadening does not in contraduction with the estimated size of the scatterers.

The obtained results provide the possibility to estimate the number and size of fluctuations of a given type, and, therefore, the fraction of the crystal volume occupied by these fluctuations. For fluctuations of size $n=30$ at $\bar{p}=0.2$, only about 1% of the whole volume is occupied by fluctuations of the given kind. This value is insufficient to form complexes due to an overlapping of neighboring fluctuations of this kind, and most of these fluctuations remain spatially isolated. This justifies a multiple-scattering approach to the lattice motion used in our consideration.

V. CONCLUSION

To summarize, a comprehensive study of the behavior of all optical-phonon modes in Raman spectra of hexagonal $Al_xGa_{1-x}N$ alloys has been carried out. It has been found that the Raman spectra of the alloys can be treated in terms of the same types of lattice vibrations as in regular crystals. The one-mode behavior of the A_1(LO) and E_1(LO) phonons and the two-mode behavior of the E_2(high), E_1(TO), and A_1(TO) phonons has been confirmed and traced in detail for the entire composition range. The two-mode behavior of the E_2(low) phonon has been revealed by Raman spectroscopy. It has been that the obtained composition dependences of the A_1(TO), A_1(LO), E_1(LO), and E_2(low) phonon energies comprise convenient tools for the quantitative characterization of the Al content in $Al_xGa_{1-x}N$ alloys.

A detailed analysis of the second-order Raman spectra has revealed a narrow gap separating the dispersion regions of transverse and longitudinal optical phonons in the phonon

DOS of alloys. A correlation between the dip in the first-order spectra in the 690–700-cm^{-1} range and the gap between the dispersion regions of transverse and longitudinal optical phonons was found. The energy position of the B_1(high) silent mode has been proposed from an analysis of the first- and second-order Raman spectra of $Al_xGa_{1-x}N$ alloys. The observed behavior for optical phonons is qualitatively consistent with the theoretical predictions given in the literature.

Experimental data have been obtained for the composition dependence of the phonon line broadening, and a theoretical analysis of this effect has been performed. It has been shown that broadening is a complex function of the composition and is caused by elastic scattering of phonons by the composition fluctuations. A theoretical approach has been used, where the statistical and dynamical aspects of the phonon scattering are treated separately. The type, size, and number of the fluctuations responsible for the phonon line broadening has been estimated. This theory, using the statistical approach, is qualitatively consistent with the experimental broadening dependences.

ACKNOWLEDGMENTS

The authors are grateful to M. V. Baidakova, M. P. Scheglov, and V. V. Tretyakov for x-ray and EPMA measurements. This work was supported by RFBR (Grant Nos. 99-02-18318 and 00-02-16999), the Program ''Physics of Solid State Nanostructures,'' and CRDF Grant No. RP1-2258.

*Author to whom correspondence should be addressed. Electronic address: valery.davydov@pop.ioffe.rssi.ru

[1] *Gallium Nitrides I*, edited by J. I. Pankove and T. Moustakas, Semiconductors and Semimetals, Vol. 50 (Academic, San Diego, CA, 1998).
[2] B. Velicky, S. Kirkpatrick, and H. Ehrenreich, Phys. Rev. **175**, 745 (1968).
[3] R.J. Elliott, J.A. Krumhansl, and P.L. Leath, Rev. Mod. Phys. **46**, 465 (1974).
[4] I.F. Chang and S.S. Mitra, Phys. Rev. **172**, 924 (1968).
[5] I.F. Chang and S.S. Mitra, Adv. Phys. **20**, 359 (1971), (and references therein).
[6] D.N. Talwar and T.D. Fang, Phys. Rev. B **41**, 3746 (1990).
[7] S.G. Yu, K.W. Kim, L. Bergman, M. Dutta, M.A. Stroscio, and J.M. Zavada, Phys. Rev. B **58**, 15 283 (1998).
[8] F. Bechstedt and H. Grille, Phys. Status Solidi B **216**, 761 (1999).
[9] H. Grille, Ch. Schnittler, and F. Bechstedt, Phys. Rev. B **61**, 6091 (2000).
[10] C. Bungaro and S. de Gironcoli, Appl. Phys. Lett. **76**, 2101 (2000).
[11] A. Cros, H. Angerer, R. Handschuh, O. Ambacher, and M. Stutzmann, Solid State Commun. **104**, 35 (1997).
[12] F. Demangeot, J. Groenen, J. Frandon, M.A. Renucci, O. Briot, S. Clur, and R.L. Aulombard, Appl. Phys. Lett. **72**, 2674 (1998).
[13] P. Wisniewski, W. Knap, J.P. Malzac, J. Camassel, M.D. Bremser, R.F. Davis, and T. Suski, Appl. Phys. Lett. **73**, 1760 (1998).
[14] M. Schubert, A. Kasic, T.E. Tiwald, J. Off, B. Kuhn, and F. Scholz, MRS Internet J. Nitride Semicond. Res. **4**, 11 (1999).
[15] N. Wieser, O. Ambacher, H. Angerer, R. Dimitrov, M. Stutzmann, B. Stritzker, and J.K.N. Lindner, Phys. Status Solidi B **216**, 807 (1999).
[16] A.A. Klochikhin, V.Yu. Davydov, I.N. Goncharuk, A.N. Smirnov, A.E. Nikolaev, M.V. Baidakova, J. Aderhold, J. Graul, J. Stemmer, and O. Semchinova, Phys. Rev. B **62**, 2522 (2000).
[17] L.K. Teles, J. Furthmüller, L.M.R. Scolfaro, J.R. Leite, and F. Bechstedt, Phys. Rev. B **62**, 2475 (2000).
[18] A. A. Maradudin, E. W. Montroll, G. N. Weiss, *Theory of Lattice Dynamics in the Harmonic Approximation* (Academic Press, New York, 1963).
[19] A.A. Maradudin, Rep. Prog. Phys. **XXVIII**, 331 (1965).
[20] A.A. Maradudin, Solid State Phys. **18**, 273 (1966); **19**, 1 (1966).
[21] L. Bergman, M.D. Bremser, W.G. Perry, R.F. Davis, M. Dutta, and R.J. Nemanich, Appl. Phys. Lett. **71**, 2157 (1997).
[22] V. Yu. Davydov, A. A. Klochikhin, I. N. Goncharuk, N. Smirnov, A. E. Nikolaev, A. S. Usikov, W. V. Lundin, M. V. Baidakova, J. Aderhold, J. Stemmer, and O. Semchinova, in *Proceedings of International Workshop on Nitride Semiconductors*, IPAP Conf. Series No 1 (Institute of Pure and Applied Physics, Tokyo, 2000), p. 657.
[23] V.Yu. Davydov, I.N. Goncharuk, M.V. Baidakova, A.N. Smirnov, A.V. Subashiev, J. Aderhold, J. Stemmer, D. Uffmann, and O. Semchinova, Mater. Sci. Eng., B **59**, 222 (1999).
[24] W.V. Lundin, A.S. Usikov, A.V. Sakharov, V.V. Tretyakov, D.V. Poloskin, N.N. Ledentsov, A. Hoffmann, Phys. Status Solidi A **176**, 379 (1999).
[25] Yu. V. Melnik, A. E. Nikolaev, S. I. Stepanov, A. S. Zubrilov, I. P. Nikitina, K. V. Vassilevski, D. V. Tsvetkov, A. I. Babanin, Yu. G. Musikhin, V. V. Tretyakov, and V. A. Dmitriev, in *Nitride Semiconductors*, edited by F. A. Ponve, S. D. Den Baars, B. K. Meyer, S. Nakamura, and S. Strite, MRS Symposia Proceedings No. 482 (Materials Research Society, Pittsburgh, 1998), p. 245.
[26] C.A. Arguello, D.L. Rousseau, and S.P.S. Porto, Phys. Rev. **181**, 1351 (1969).
[27] T. Azuhata, T. Sota, K. Suzuki, and S. Nakamura, J. Phys.: Condens. Matter **7**, L129 (1995).
[28] L. Filippidis, H. Siegle, A. Hoffmann, C. Thomsen, K. Karch, and F. Bechstedt, Phys. Status Solidi B **198**, 621 (1996).
[29] V.Yu. Davydov, Yu.E. Kitaev, I.N. Goncharuk, A.N. Smirnov, J. Graul, O. Semchinova, D. Uffmann, M.B. Smirnov, A.P. Mirgorodsky, and R.A. Evarestov, Phys. Rev. B **58**, 12 899 (1998).
[30] L.E. McNail, M. Grimsditch, and R.H. French, J. Am. Ceram. Soc. **76**, 1132 (1993).
[31] J.M. Hayes, M. Kuball, Y. Shi, and J.H. Edgar, Jpn. J. Appl. Phys., Part 2 **39**, L710 (2000).
[32] T. Kozawa, T. Kachi, H. Kano, Y. Taga, M. Hachimoto, N. Koide, and K. Manabe, J. Appl. Phys. **75**, 1098 (1993).
[33] H. Harima, H. Sakashita, T. Inoue, and S. Nakashima J. Cryst. Growth **189/190**, 672 (1997).
[34] M. Holz, T. Prokofyeva, M. Seon, K. Copeland, J. Vanbuskirk, S. Williams, S.A. Nikishin, V. Tretyakov, and H. Temkin, J. Appl. Phys. **89**, 7977 (2001).
[35] J.C. Nipko and C.-K. Loong, Phys. Rev. B **57**, 10 550 (1998).
[36] J.C. Nipko, C.-K. Loong, C.M. Balkas, and R.F. Davis, Appl. Phys. Lett. **73**, 34 (1998).

[37] K. Shimada, T. Sota, and K. Suzuki, J. Appl. Phys. **84**, 4951 (1998).
[38] M. Schwöerer-Bohning, A.T. Macrander, M. Pabst, and P. Pavone, Phys. Status Solidi B **215**, 177 (1999).
[39] J.M. Zhang, T. Ruf, M. Cardona, O. Ambacher, M. Stutzmann, J.-M. Wagner, and F. Bechstedt, Phys. Rev. B **56**, 14 399 (1997).
[40] K. Karch, J.M. Wagner, and F. Bechstedt, Phys. Rev. B **57**, 7043 (1998).
[41] C. Bungaro, K. Rapcewicz, and J. Bernholc, Phys. Rev. B **61**, 6720 (2000).
[42] T. Ruf, J. Serrano, M. Cardona, P. Pavone, M. Pabst, M. Krisch, M. D'Astuto, T. Suski, I. Grzegory, and M. Leszczynski, Phys. Rev. Lett. **86**, 906 (2001).
[43] K. Karch and F. Bechstedt, Phys. Rev. B **56**, 7404 (1997).
[44] M. Cardona, in *Light Scattering in Solids II*, edited by M. Cardona and G. Guntherodt, Topic in Applied Physics Vol. 50 (Springer, Berlin, 1982), p. 117.
[45] M. Lannoo and P. Lenglart, J. Phys. Chem. Solids **30**, 2409 (1969).
[46] J. Bernholc and S.T. Pantelides, Phys. Rev. B **18**, 1780 (1978).
[47] J.W. Essam, in *Phase Transitions and Critical Phenomena, Vol. 2: Percolation and Cluster Size*, edited by C. Domb and M.S. Green (Academic Press, London, 1972), p. 197.
[48] J.W. Essam, Rep. Prog. Phys. **43**, 833 (1980).
[49] A. Bunde and S. Havlin, in *Fractals and Disordered Systems*, edited by. A. Bunde and S. Havlin (Springer-Verlag, Berlin, 1994), p. 51.
[50] M.F. Sykes, D.S. Gaunt, and M. Glen, J. Phys. A **9**, 1705 (1976).